Electronic Supplementary Material (ESI) for Inorganic Chemistry Frontiers.
This journal is © the Partner Organisations 2024

Tailoring supertetrahedral cadmium/tin selenide clusters into a robust framework for efficient elimination of Cs^{+}, Co^{2+}, and Ni^{2+} ions

Kai-Yao Wang,*[a] Meng-Yu Li,[a] Lin Cheng,[b] Xin Hao,[a] and Cheng Wang[a]

[a]Tianjin Key Laboratory of Advanced Functional Porous Materials, Institute for New Energy Materials & Low-Carbon Technologies, School of Materials Science and Engineering, Tianjin University of Technology, Tianjin 300384, P.R. China.

[b]College of Chemistry, Tianjin Normal University, Tianjin 300387, P.R. China.

*Corresponding Author: Kai-Yao Wang. Email: kaiyao0729@163.com.

Supporting Information Content:

Number of Figures: 26 (Figure S1 to Figure S26).

Number of Tables: 14 (Table S1 to Table S14).

Section 1 Synthesis and Structure

Table S1. Crystal data for **CdSnSe-2**.

Compound	**CdSnSe-2**
Empirical formula	$C_4H_{22}Cd_2N_4Se_{10}Sn_3$
Formula weight	1484.71
Crystal system	Tetragonal
Space group	$I\bar{4}$
T/K	293(2) K
λ/Å	1.54178
a/Å	9.7043(4)
b/Å	9.7043(4)
c/Å	16.0699(17)
α/°	90
β/°	90
γ/°	90
V/Å^3	1513.4(2)
Z	2
D_c/Mg m^{-3}	3.258
μ/mm^{-1}	44.243
F(000)	1308
Measured refls.	2212
Independent refls.	1314
R_{int}	0.0354
No. of parameters	57
GOF	1.009
R_1,[a] $wR_2[I > 2\sigma(I)]$	0.0495, 0.1381
R_1, wR_2 (all data)	0.0514, 0.1395

[a] $R_1 = \sum||F_o|-|F_c||/\sum|F_o|$, $wR_2 = \{\sum w[(F_o)^2 -(F_c)^2]^2/\sum w[(F_o)^2]^2\}^{1/2}$

Table S2. Selected hydrogen-bonding data for **CdSnSe-2**.

D–H···A	*d*(D–H)	*d*(H···A)	*d*(D···A)	<(DHA)
N(2)–H(2A)···N(1)	0.90	2.39	3.16(3)	144.4
N(2)–H(2B)···Se(3)#4	0.90	2.92	3.54(3)	126.7
N(2)–H(2C)···Se(2)#6	0.90	2.84	3.70(3)	160.3
C(2)–H(2D)···Se(2)#7	0.96	2.83	3.79(3)	175.0
C(2)–H(2E)···Se(2)	0.96	3.14	3.78(3)	125.3
C(2)–H(2F)···Se(1)#4	0.96	3.02	3.92(3)	154.9

Symmetry transformations used to generate equivalent atoms: #1 *y*, -*x*+2, -*z*+2; #2 -*y*+3/2, *x*-1/2, -*z*+3/2; #3 -*x*+2, -*y*+1, *z* ; #4 *y*+1/2, -*x*+3/2, -*z*+3/2; #5 -*x*+2, -*y*+2, *z*; #6 -*y*+2, *x*, -*z*+2; #7 *y*+1, -*x*+2, -*z*+2.

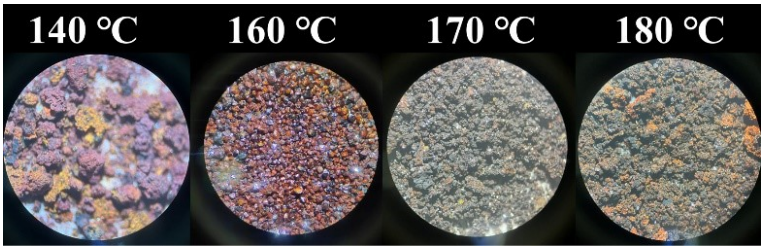

Figure S1. Photographs of the products obtained from the optimizing reactions for **CdSnSe-2** performed at different temperatures.

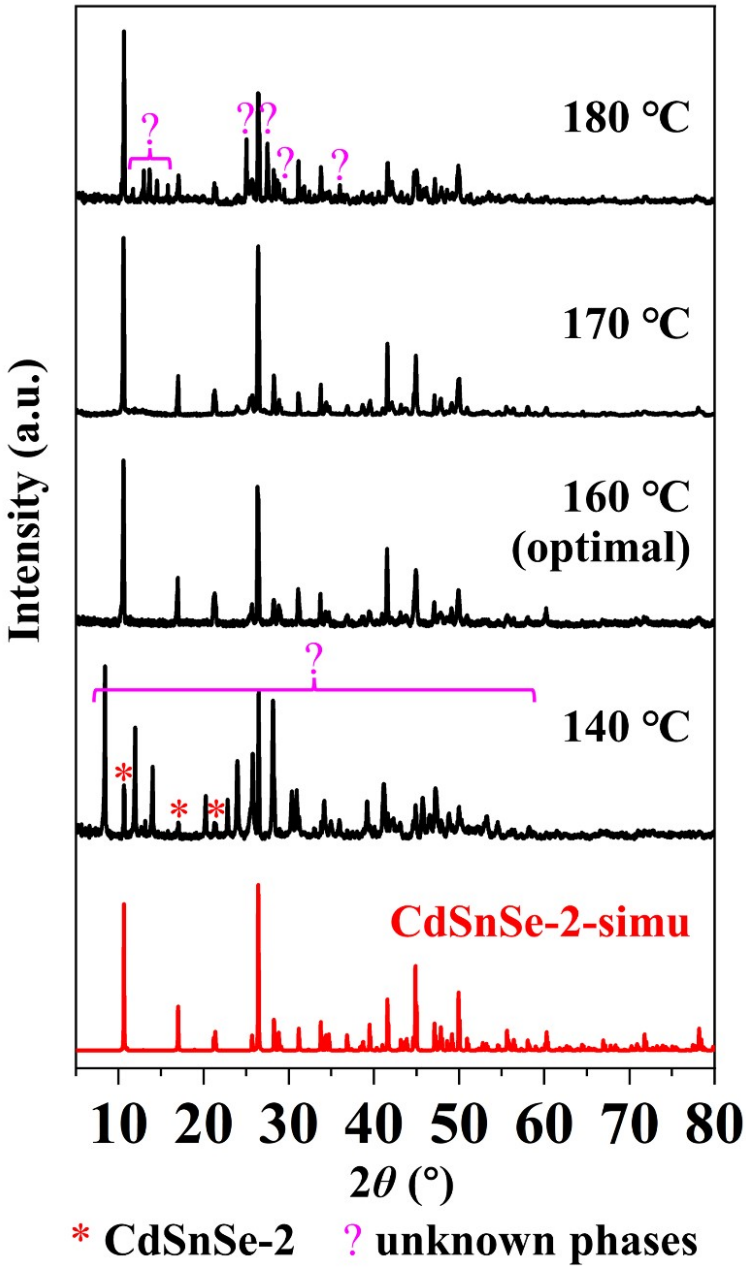

Figure S2. Powder XRD patterns of the products obtained from the optimizing reactions for **CdSnSe-2** performed at different temperatures.

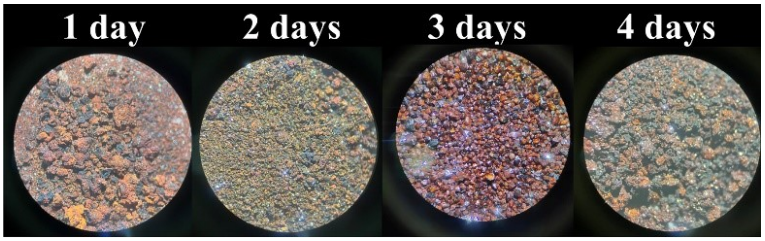

Figure S3. Photographs of the products obtained from the optimizing reactions for **CdSnSe-2** with different time at 160 °C.

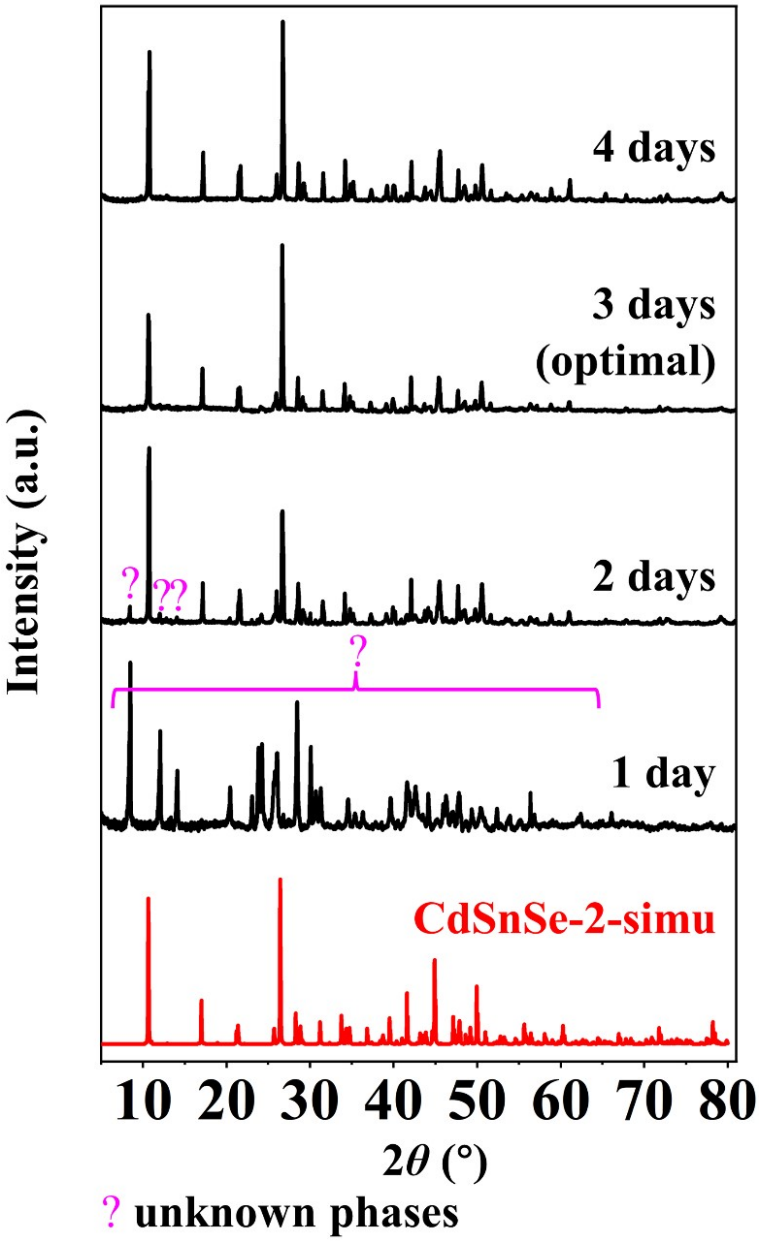

Figure S4. Powder XRD patterns of the products obtained from the optimizing reactions for **CdSnSe-2** with different time at 160 °C.

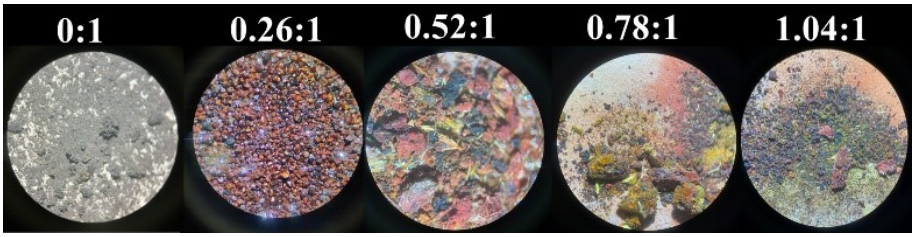

Figure S5. Photographs of the products obtained from the optimizing reactions for **CdSnSe-2** with different $N_2H_4 \cdot H_2O$:N,N'-dimethylurea molar ratios at 160 °C. The initial amount of N,N'-dimethylurea is 16 mmol.

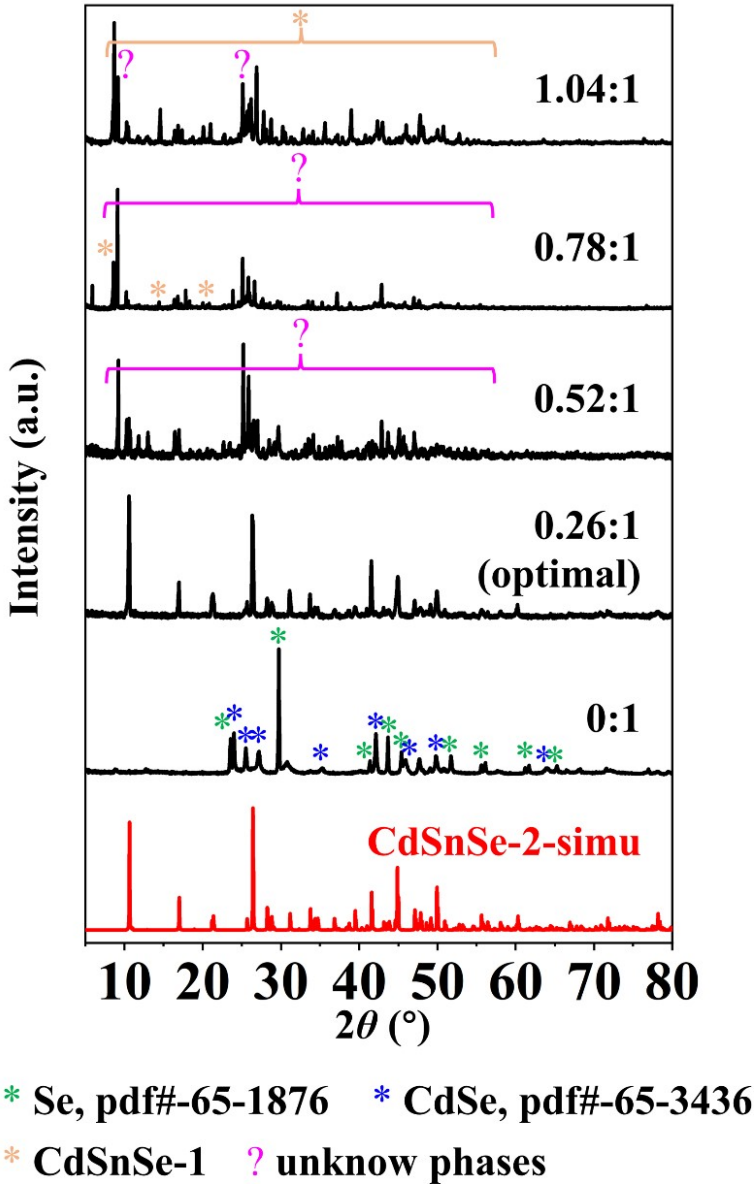

Figure S6. Powder XRD patterns of the products obtained from the optimizing reactions for **CdSnSe-2** with different $N_2H_4 \cdot H_2O$:N,N'-dimethylurea molar ratios at 160 °C. The initial amount of N,N'-dimethylurea is 16 mmol.

Figure S7. Photographs of the products obtained from the optimizing reactions for **CdSnSe-2** with different alkylamine hydrochlorides at 160 °C.

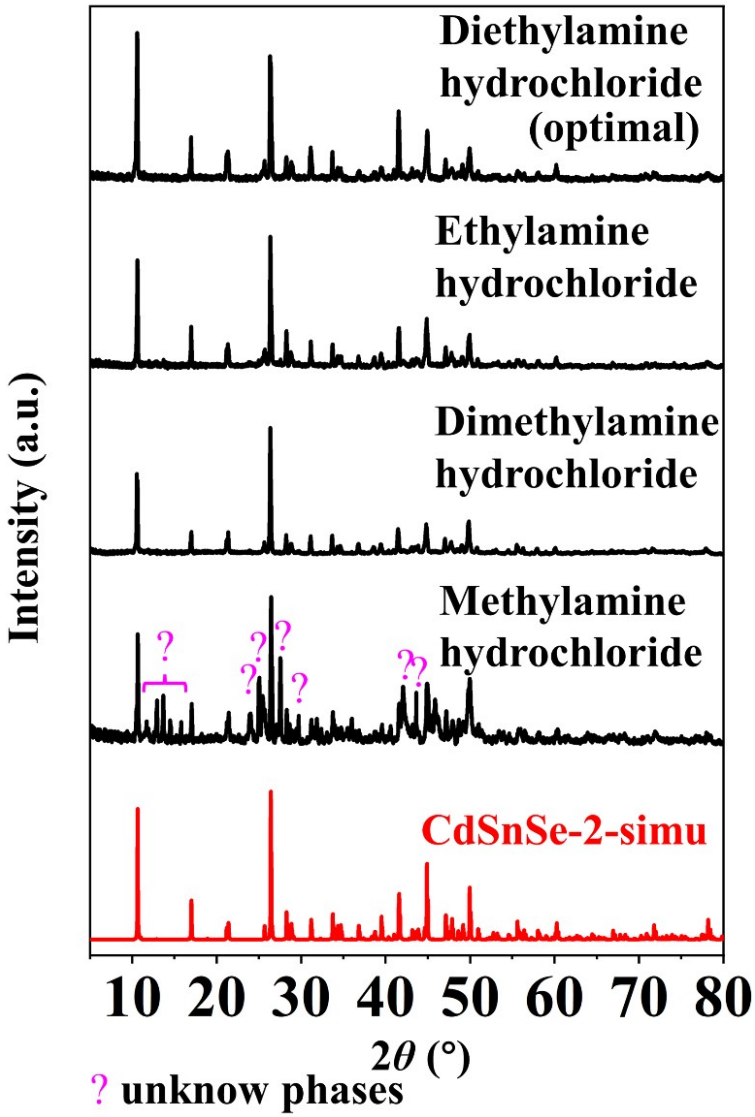

Figure S8. Powder XRD patterns of the products obtained from the optimizing reactions for **CdSnSe-2** with different alkylamine hydrochlorides at 160 °C.

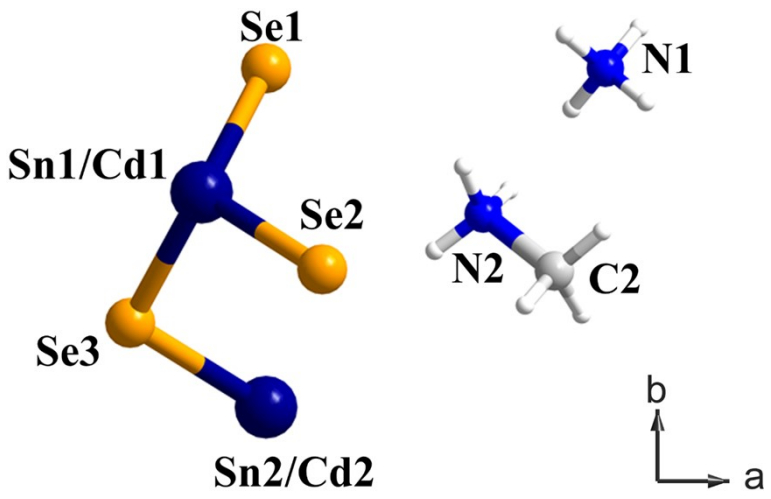

Figure S9. The asymmetric unit of **CdSnSe-2**.

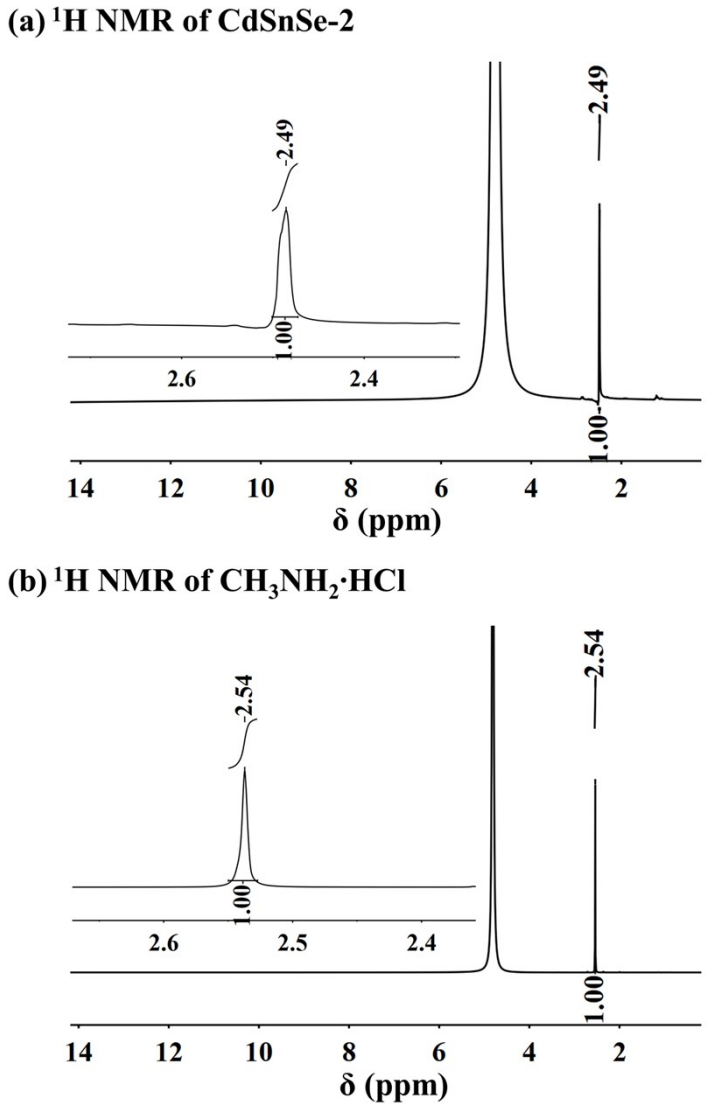

Figure S10. ^{1}H NMR spectra of (a) **CdSnSe-2** and (b) $CH_3NH_2 \cdot HCl$.

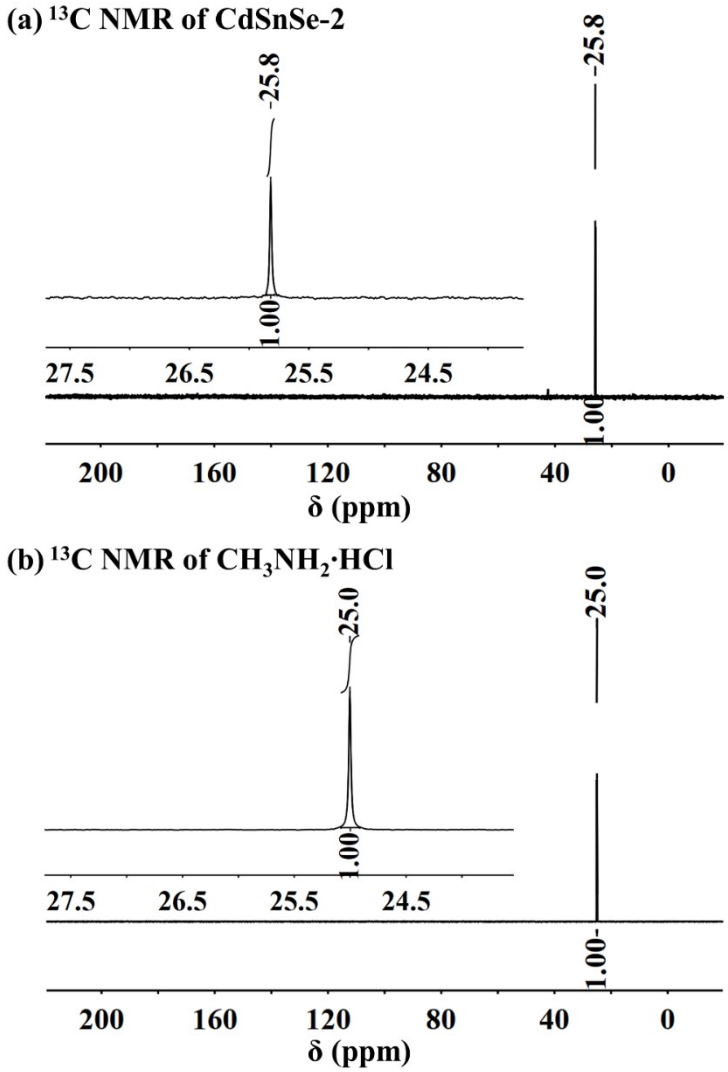

Figure S11. ^{13}C NMR spectra of (a) **CdSnSe-2** and (b) $CH_3NH_2 \cdot HCl$.

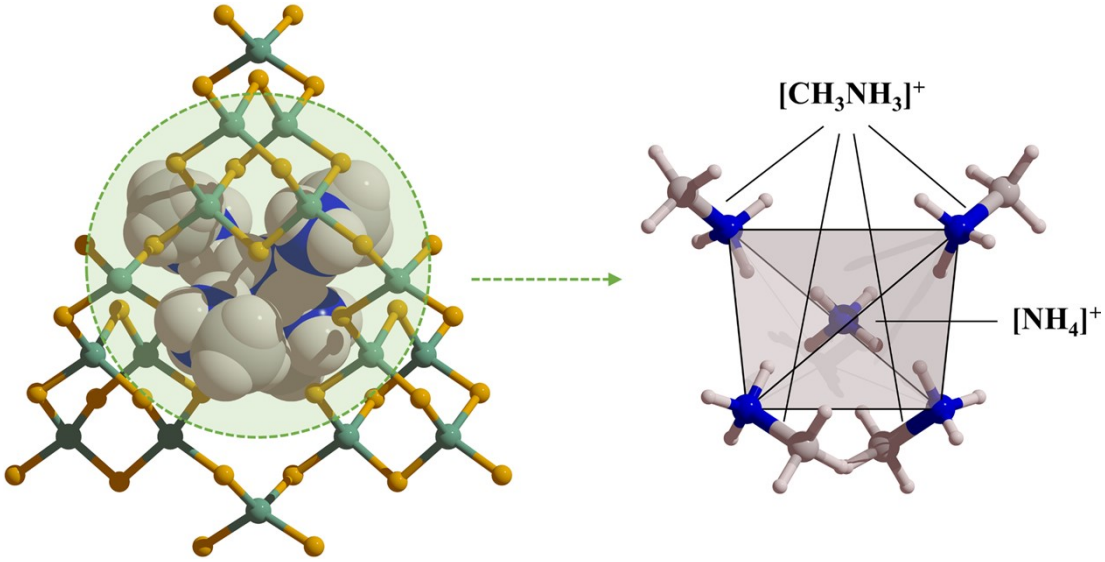

Figure S12. Positional relationship between the ammonium and methylammonium cations in the anionic framework of **CdSnSe-2** viewed along the a axis.

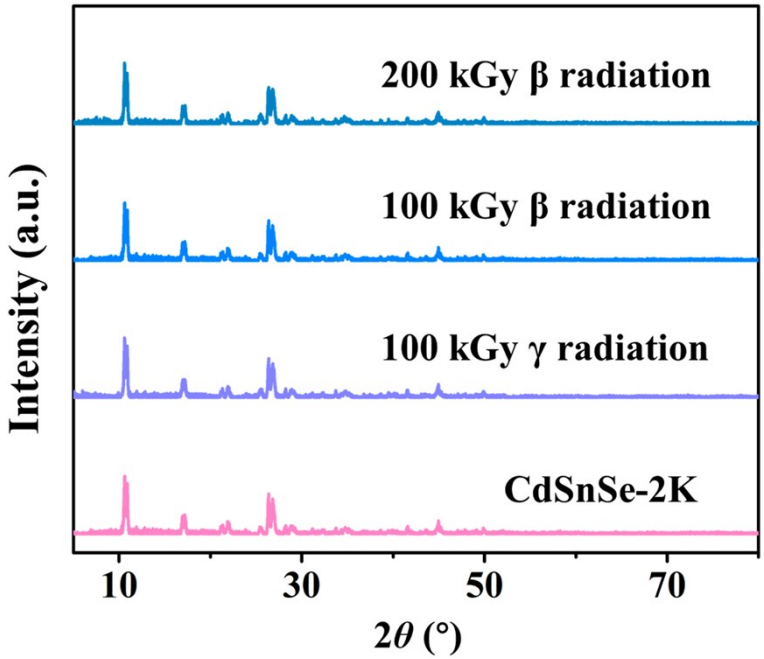

Figure S13. Powder XRD patterns of **CdSnSe-2K** and the corresponding samples after β and γ irradiations.

Table S3. Molecular formulae and weight losses of **CdSnSe-2** and **CdSnSe-2K**, **CdSnSe-2Cs**, **CdSnSe-2Co** and **CdSnSe-2Ni**.

Products	**Molecular Formula**	**Weight loss (%)** **40-150** °C
CdSnSe-2	$(CH_3NH_3)_3NH_4Cd_2Sn_3Se_{10}$	-0.02%
CdSnSe-2K	$K_{3.4}(CH_3NH_3)_{0.45}(NH_4)_{0.15}Cd_2Sn_3Se_{10}\cdot 3.4H_2O$	-3.63%
CdSnSe-2Cs	$Cs_{2.46}K_{0.94}(CH_3NH_3)_{0.45}(NH_4)_{0.15}Cd_2Sn_3Se_{10}\cdot 0.4H_2O$	-0.40%
CdSnSe-2Co	$Co_{1.02}K_{1.36}(CH_3NH_3)_{0.45}(NH_4)_{0.15}Cd_2Sn_3Se_{10}\cdot 1.2H_2O$	-1.42%
CdSnSe-2Ni	$Ni_{0.85}K_{1.7}(CH_3NH_3)_{0.45}(NH_4)_{0.15}Cd_2Sn_3Se_{10}\cdot 1.6H_2O$	-1.85%

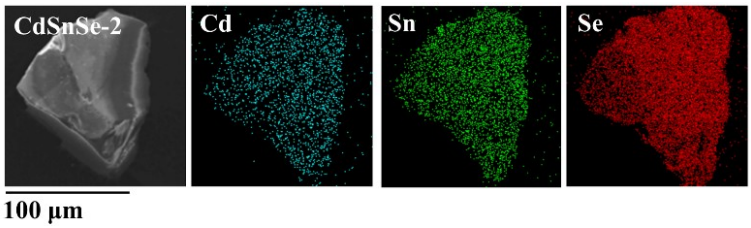

Figure S14. SEM and elemental mapping images of **CdSnSe-2**.

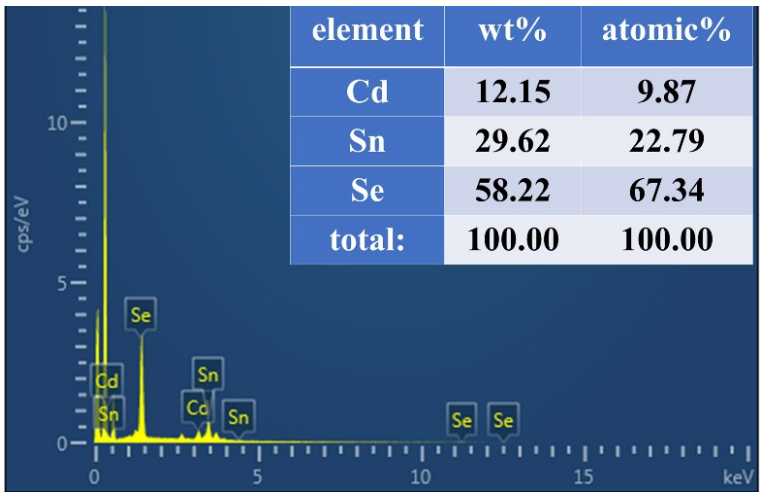

element	wt%	atomic%
Cd	12.15	9.87
Sn	29.62	22.79
Se	58.22	67.34
total:	100.00	100.00

Figure S15. EDS analysis on **CdSnSe-2**.

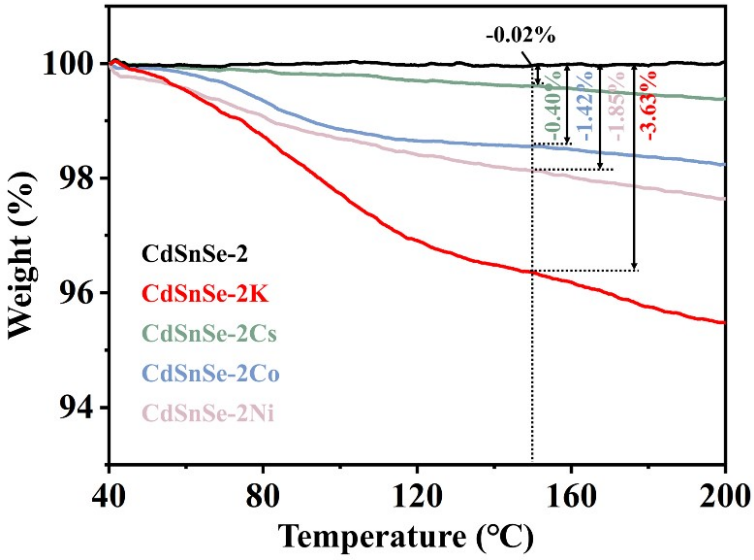

Figure S16. Thermogravimetric curves of **CdSnSe-2**, **CdSnSe-2K**, **CdSnSe-2Cs**, **CdSnSe-2Co** and **CdSnSe-2Ni**.

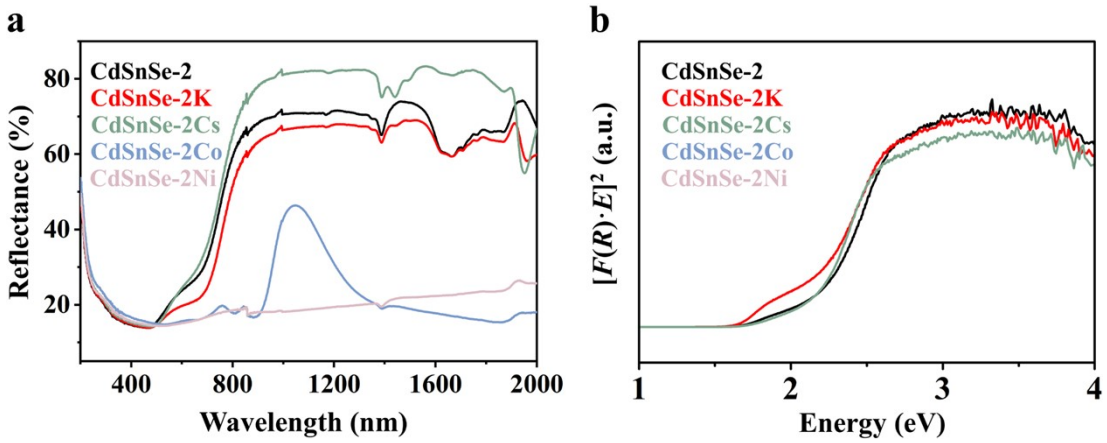

Figure S17. (a) Solid-state UV-vis reflectance spectra of **CdSnSe-2**, **CdSnSe-2K**, **CdSnSe-2Cs**, **CdSnSe-2Co** and **CdSnSe-2Ni**. (b) Kubelka-Munk spectra of **CdSnSe-2**, **CdSnSe-2K** and **CdSnSe-2Cs**.

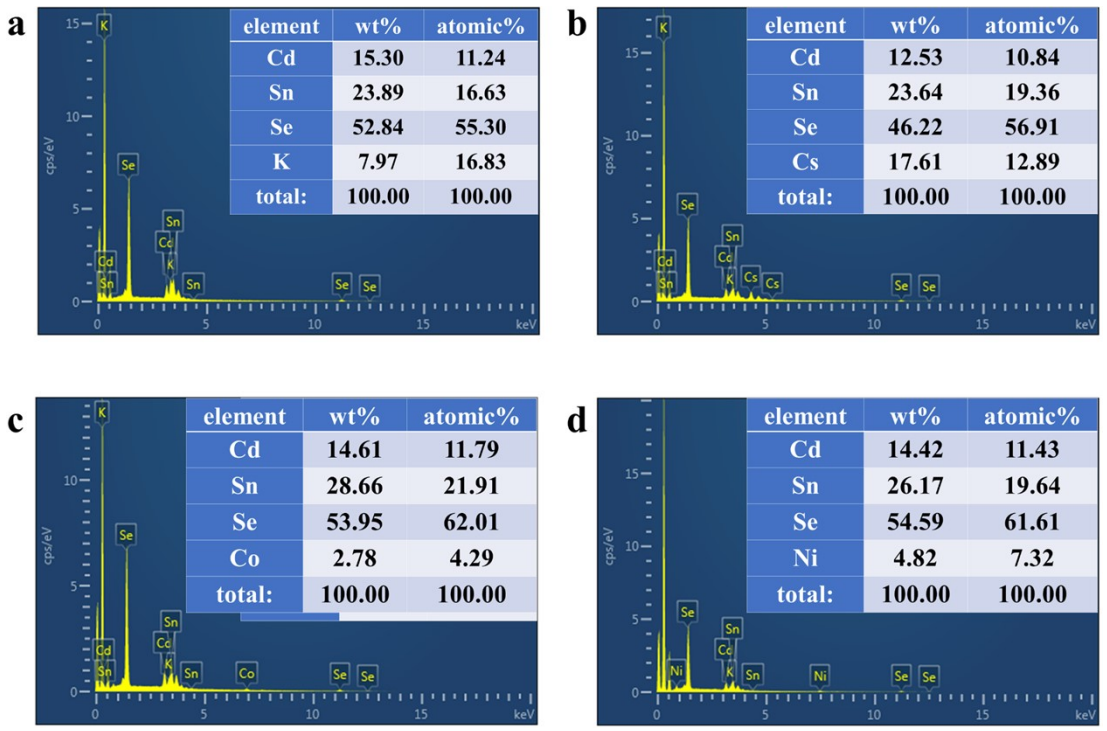

Figure S18. EDS analyses on (a) **CdSnSe-2K**, (b) **CdSnSe-2Cs**, (c) **CdSnSe-2Co** and (d) **CdSnSe-2Ni**.

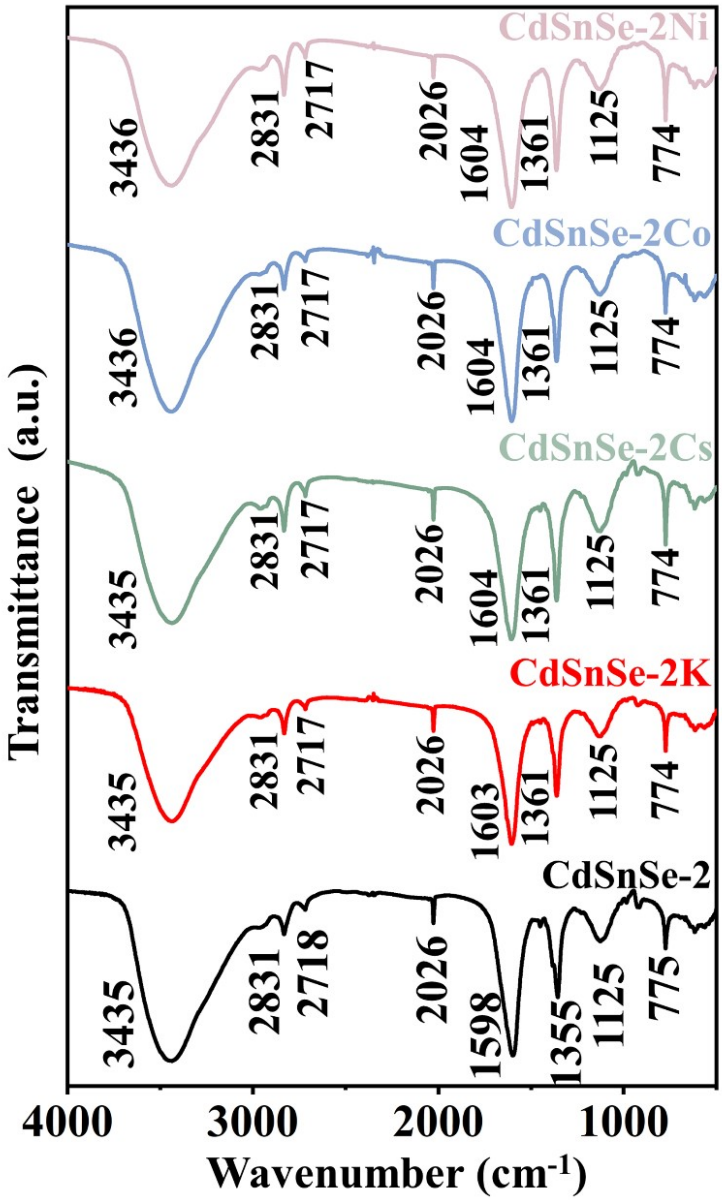

Figure S19. FTIR spectra of **CdSnSe-2**, **CdSnSe-2K**, **CdSnSe-2Cs**, **CdSnSe-2Co** and **CdSnSe-2Ni** measured at room temperature on KBr pellets.

Section 2 Adsorption kinetics and isotherms

Table S4. The concentrations of Cs^{+}, Co^{2+} and Ni^{2+} (C_t^{Cs}, C_t^{Co}, C_t^{Ni}, ppm) and the corresponding removal rates (R^{Cs}, R^{Co}, R^{Ni}, %) at different contact time t (min) in kinetic experiments.

t (min)	C_t^{Cs} (ppm)	R^{Cs} (%)	C_t^{Co} (ppm)	R^{Co} (%)	C_t^{Ni} (ppm)	R^{Ni} (%)
0	6.1480	0	5.7624	0	5.5760	0
0.5	0.2735	95.551	/	/	/	/
1	0.133	97.837	/	/	/	/
2	0.0895	98.544	2.2050	61.735	3.1205	44.037
5	0.0265	99.569	0.9978	82.685	1.6078	71.167
10	0.0223	99.638	0.4170	92.763	0.7518	86.518
20	0.0210	99.658	0.1448	97.488	0.3580	93.580
40	0.0335	99.455	0.1228	97.870	0.1298	97.673
60	0.0190	99.691	0.1073	98.139	0.1358	97.565
80	/	/	0.1060	98.160	0.1223	97.808
120	0.0278	99.549	0.0968	98.321	0.1223	97.808
240	0.0450	99.268	0.0570	99.011	0.0710	98.727

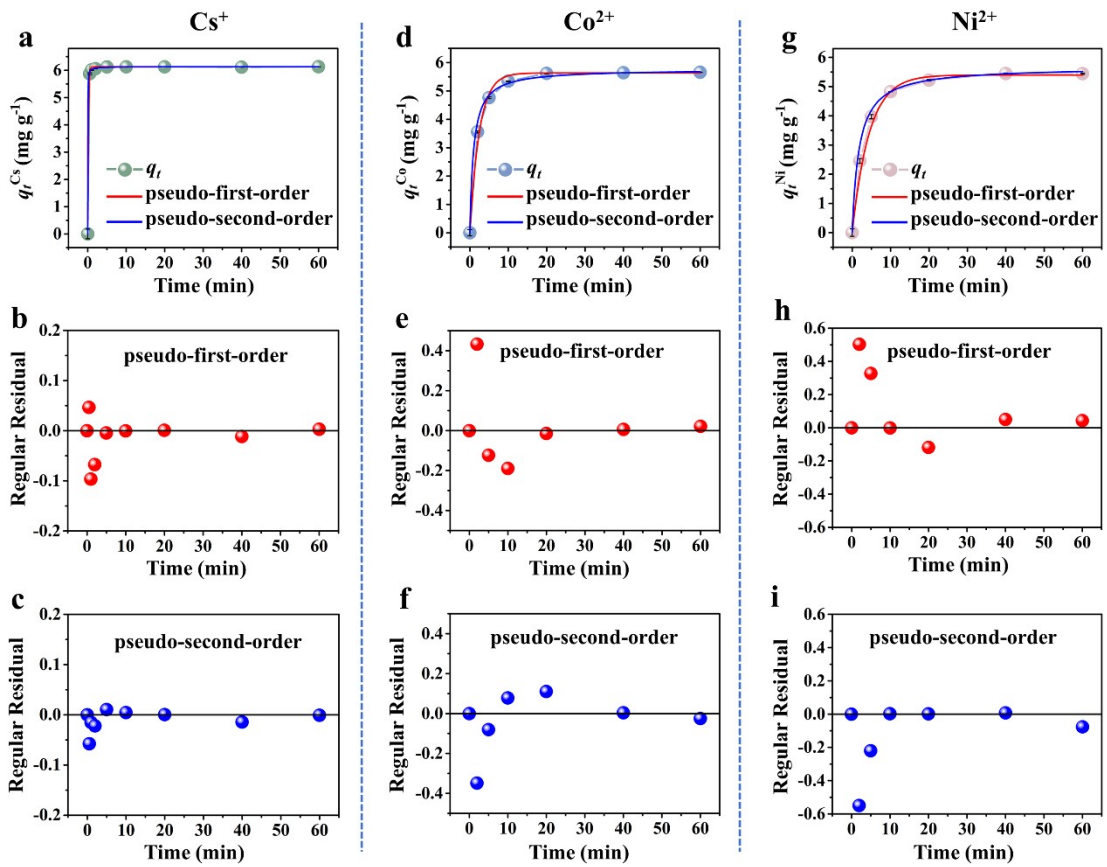

Figure S20. Non-linear Fitting of the kinetic data and the corresponding regular residuals for (a,b,c) Cs^+, (d,e,f) Co^{2+}, and (g,h,i) Ni^{2+} ions by using pseudo-fisrt-order and pseudo-second-order models.

Table S5. The parameters calculated for the fitting of Cs^+, Co^{2+} and Ni^{2+} adsorption kinetics by **CdSnSe-2K** using the non-linear pseudo-first-order and pseudo-second-order model (within 60 min contact time).

ions	$q_{e,exp}$ (mg g^{-1})	$q_{e,cal}$ (mg g^{-1})	k_1 (min^{-1})	k_2 (g mg^{-1} min^{-1})	R^2
pseudo-first-order					
Cs^+	6.122	6.126	6.046	–	0.73607
Co^{2+}	5.705	5.633	0.404	–	0.92873
Ni^{2+}	5.505	5.397	0.225	–	0.97593
pseudo-second-order					
Cs^+	6.122	6.132	–	9.706	0.92807
Co^{2+}	5.705	5.770	–	0.182	0.95344
Ni^{2+}	5.505	5.681	–	0.099	0.98282

Table S6. Comparison of the initial Cs^+ concentration (C_0^{Cs}), removal rate (R_e^{Cs}) and time (t_e) at equilibrium, and pseudo-second-order adsorption rate constant (k_2) for **CdSnSe-2K** and other inorganic adsorbents.

Adsorbents	C_0^{Cs} **(ppm)**	R_e^{Cs}	t_e **(min)**	k_2 **(g mg^{-1} min^{-1})**	**Ref.**
CdSnSe-2K	6	99.569% (1 min/97.837%)	≤5	9.706	This work
ZnSnSe-1K	6	99.34%	2	9.240	[1]
SbS-1K	6	99.06%	40	1.040	[2]
InSnS-1	3.44	95-96%	>60	1.77846	[3]
PIATS	34	99%	3	0.25	[4]
K-MPS-1	45	77.6%	15	0.0982	[5]
FJSM-SnS/PAN	9.32	80.17%	180	0.0314	[6]
KMS-1	1	>90%	5	NA	[7]
KTS-3	1.2	94%	5	NA	[8]
KIAS	2.05	95%	10	NA	[9]
FJSM-SnS	130.4	55%	30	NA	[10]
FJSM-SnS-2	0.73	83%	60	NA	[11]
FJSM-SnS-3	0.778	75%	60	NA	
FJSM-SnS-4	11.2	78.57%	30	-0.1189	[12]
FJSM−SbS	0.6	86.9%	2	NA	[13]

FJSM-InMOF	90.7	95.259%	>300	NA	[14]
$[(CH_3)_2NH_2]In(aip)_2 \cdot DMF \cdot H_2O$	6.5	NA	5	NA	[15]
$[(CH_3)_2NH_2]In(hip)_2 \cdot DMF \cdot H_2O$	3.9	NA	10	NA	
InSnOS	1	97%	5	NA	[16]
$[MeNH_3]_{5.5}[Me_2NH_2]_{0.5}In_{10}S_{18} \cdot 7H_2O$	6.13	92%	5	NA	[17]
$[Me_2NH_2]_6In_{10}S_{18}$	5.73	74%	5	NA	
Zeolite A	100	69%	90-120	1.5×10^{-3}	[18]
ZTP	6	≈ 76%	60	0.253	[19]
$Fe_3O_4@WO_3$	100	52.92%	180	0.1423	[20]
mag-AMP	75	82.88%	5	0.06914	[21]
NiSiO@NiAlFe LDHs	20	NA	20	0.023	[22]
mag-Nb-CST	0.1	49.05%	180	0.014	[23]
$Ti_3C_2T_x$	2	≈ 80%	60	0.0126	[24]
K-SGU-45	1.3	>99%	15	NA	[25]
$NH_4V_4O_{10}$	300	65.65%	180	2.6×10^{-3}	[26]
NaFeTiO	500	NA	120	1.9×10^{-3}	[27]
APS-4	10	>95%	720	7.019×10^{-4}	[28]

Table S7. The parameters calculated for the fitting of Cs^+, Co^{2+} and Ni^{2+} adsorption isotherms by **CdSnSe-2K** using Langmuir-Freundlich models.

Model	q_m **(mg g^{-1})**	b **(L mg^{-1})**	n	R^2
Cs^+	218.08 ± 80.08	0.00673 ± 0.01293	2.332 ± 0.576	0.98204
Co^{2+}	43.95 ± 16.57	0.0046 ± 0.01252	3.58 ± 0.878	0.96958
Ni^{2+}	42.527 ± 16.50	0.11743 ± 0.31218	2.67 ± 1.51	0.90573

Table S8. M:Cd (M = Cs, Co, Ni) molar ratio and the calculated M^{n+} adsorption capacities of the exchanged products obtained from solutions with C_0^M varying from 0.05 to 0.2 mol L^{-1} according to ICP-MS test.

C_0^M **(mol L^{-1})**	**M:Cd molar ratio**	**Exchange capacity (mg g^{-1})**
Cs^+		
0.05	1.216:1	204.322
0.1	1.200:1	201.634
0.2	1.274:1	214.068
average	1.230:1	206.680
Co^{2+}		
0.05	0.5257:1	39.170
0.1	0.5324:1	39.660
0.2	0.4756:1	35.430
average	0.5112:1	38.090
Ni^{2+}		
0.05	0.4296:1	31.878
0.1	0.4217:1	31.291
0.2	0.4255:1	31.573
average	0.4256:1	31.581

Theoretical exchange capacities of Cs^+, Co^{2+}, Ni^{2+} and by $K_{3.4}(CH_3NH_3)_{0.45}(NH_4)_{0.15}Cd_2Sn_3Se_{10}\cdot 3.4H_2O$ (**CdSnSe-2K**, FM = 1581.87 g mol^{-1} = 1581.87 mg $mmol^{-1}$) are calculated as follows:

(1) For 1 g exchanger, the molar amount of K^+:

$n(K^+) = m/FM \times 3.4 = 1\ g/1581.87\ g\ mol^{-1} \times 3.4 = 0.0021494\ mol$

(2) If all the K^+ are replaced by Cs^+ or Sr^{2+}, the molar amount of Cs^+, Co^{2+}, Ni^{2+} should be:

$n(Cs^+) = n(K^+) = 0.0021494\ mol$

$n(Co^{2+}) = n(Ni^{2+}) = n(K^+)/2 = 0.0010747\ mol$

(3) The theoretical mass of adsorbed Cs^+, Co^{2+}, Ni^{2+} should be:

$m(Cs^+) = n(Cs^+) \times M(Cs^+) = 0.0021494\ mol \times 132.9\ g\ mol^{-1} = 0.28566\ g = 285.66\ mg$

$m(Co^{2+}) = n(Co^{2+}) \times M(Co^{2+}) = 0.0010747\ mol \times 58.93\ g\ mol^{-1} = 0.06333\ g = 63.33\ mg$

$m(Ni^{2+}) = n(Ni^{2+}) \times M(Ni^{2+}) = 0.0010747\ mol \times 58.69\ g\ mol^{-1} = 0.06307\ g = 63.07\ mg$

Section 3 Effects of solution pH on adsorption

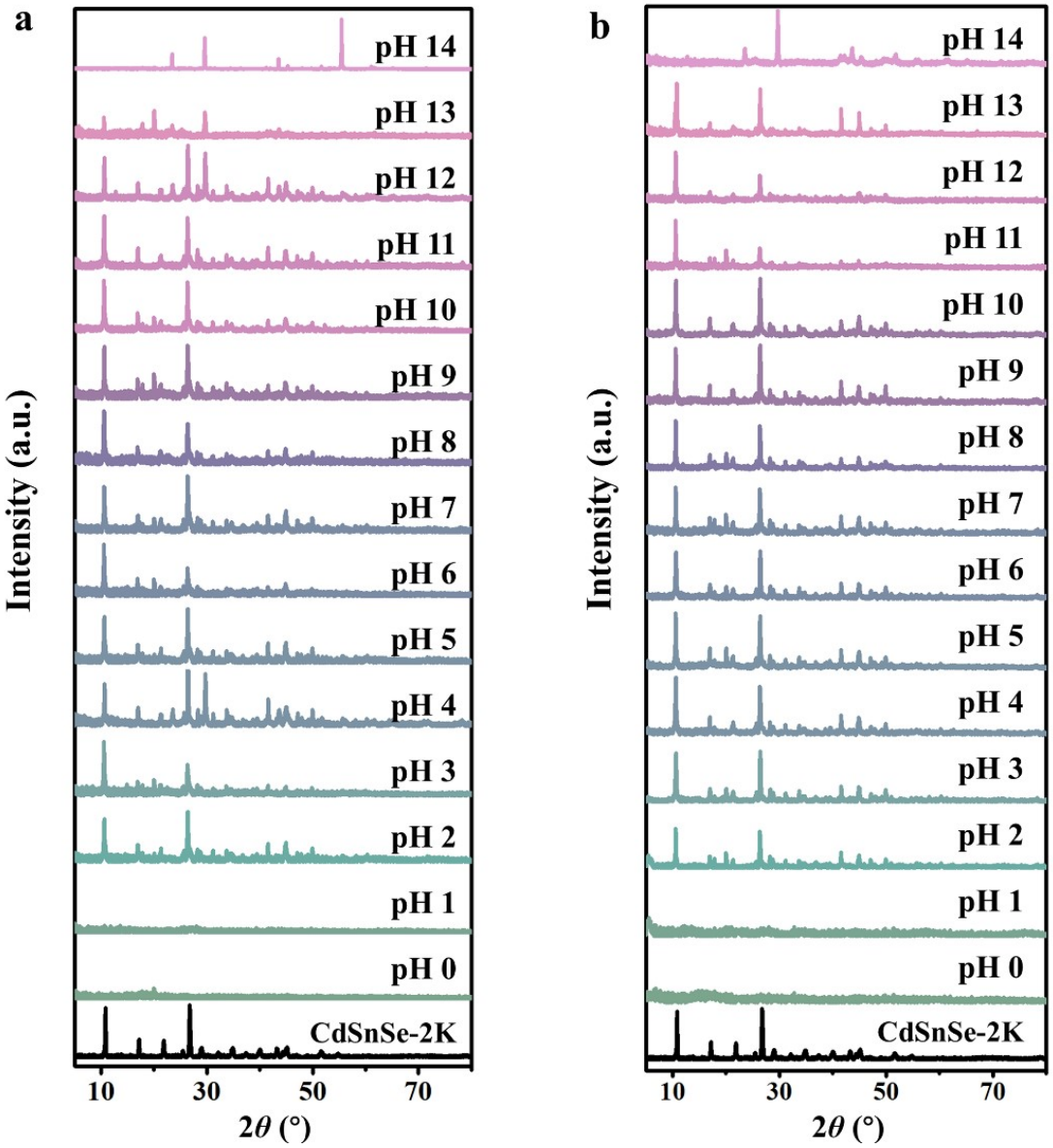

Figure S21. Powder XRD patterns of the (a) Co^{2+} and (b) Ni^{2+}exchanged products at different pH values.

Table S9. Removal rates and K_d values of individual Cs^+, Co^{2+}, Ni^{2+} ions using **CdSnSe-2K** in the pH range of 0-14 (C_0 ~ 6 ppm for Cs^+, Co^{2+}, Ni^{2+}; V/m = 1000 mL g^{-1}; room temperature)

pH	R^{Cs} (%)	K_d^{Cs} (mL g^{-1})	R^{Co} (%)	K_d^{Co} (mL g^{-1})	R^{Ni} (%)	K_d^{Ni} (mL g^{-1})
0	3.04	31.32	2.87	29.59	2.39	24.53
1	1.85	18.87	0.98	9.89	7.40	79.92
2	97.97	48224.57	20.13	252.13	6.56	70.23
3	99.02	101237.90	34.74	532.44	27.54	380.04
4	99.32	145342.70	95.01	19032.66	98.16	53457.90
5	98.47	64776.92	99.18	121561.80	98.62	71721.09
6	99.57	231000	99.01	100096.49	98.73	77535.21
7	98.99	98150.20	98.72	76896.19	98.10	51496.42
8	98.63	71902.65	98.08	51007.13	90.19	9192.42
9	98.37	60504.76	99.22	127100	97.88	46112.15
10	98.22	55188.18	99.75	404981.13	96.76	29909.49
11	64.58	1823.71	99.77	443170.21	94.49	17138.02
12	23.22	302.55	–	–	–	–
13	7.54	81.55	–	–	–	–
14	5.23	55.22	–	–	–	–

Section 4 Effect of competitive ions on adsorption

Table S10. Removal rates and K_d values for individual Cs^+, Co^{2+} and Ni^{2+} exchange with increasing concentrations of Na^+, K^+, Mg^{2+} and Ca^{2+} from 0 to 100 mmol L^{-1} (C_0 ≈ 6 ppm for Cs^+, Co^{2+} and Ni^{2+}; V/m = 1000 mL g^{-1}; room temperature).

C (mmol L^{-1})	R^{Cs} (%)	K_d^{Cs} (mL g^{-1})	R^{Co} (%)	K_d^{Co} (mL g^{-1})	R^{Ni} (%)	K_d^{Ni} (mL g^{-1})
Na^+						
0	99.57	231000	99.01	100096.49	98.73	77535.21
0.1	98.76	79462.90	98.38	60729.11	94.64	17643.88
1	98.82	83985.45	95.84	23052.40	94.31	16577.45
10	95.64	21925.43	84.61	5498.87	81.68	4457.48
100	92.29	11970.23	69.25	2251.65	75.78	3128.90
K^+						
0	99.57	231000	99.01	100096.49	98.73	77535.21
0.1	98.57	69162.24	96.76	29936.58	97.95	47697.89
1	97.07	33080.76	83.53	5072.39	98.08	51036.41
10	86.76	6552.81	77.45	3435.11	79.53	3884.71
100	63.19	1716.43	53.80	1164.77	58.48	1408.73
Mg^{2+}						
0	99.57	231000	99.01	100096.49	98.73	77535.21
0.1	98.49	65389.78	88.28	7537.44	99.23	128893.62
1	97.04	32732.22	79.09	3783.74	95.91	23421.35
10	95.32	20345.66	84.35	5390.35	86.67	6502.25
100	91.25	10429.93	65.00	1857.21	26.10	353.24
Ca^{2+}						
0	99.57	231000	99.01	100096.49	98.73	77535.21
0.1	96.20	25291.84	95.03	19120.45	98.30	57764.89
1	96.18	25200.66	85.23	5770.02	93.63	14687.99
10	86.65	6492.74	87.04	6716.94	74.15	2868.81
100	72.62	2651.91	74.12	2864.02	30.42	437.27

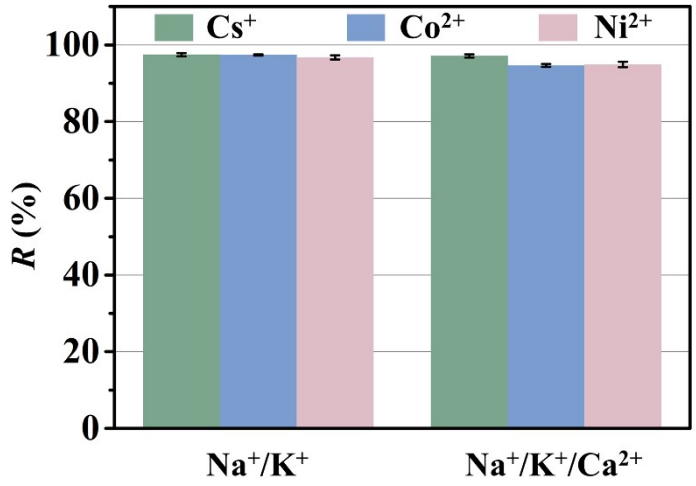

Figure S22. The removal rates of mixed Cs^+, Co^{2+} and Ni^{2+} by CdSnSe-2K in presence of mixed Na^+/K^+ and $Na^+/K^+/Ca^{2+}$. Note: C_0 = 6 ppm for each of Cs^+, Co^{2+} and Ni^{2+}; C_0 = 0.1 mmol L^{-1} for each of Na^+, K^+ and Ca^{2+}; V/m = 1000 mL g^{-1}; room temperature.

Table S11. Removal rates and K_d values for individual Cs^+, Co^{2+} and Ni^{2+} adsorption experiments performed in deionized water (DW), mineral water (MW), tap water (TW), lake water (LW) and sea water (SW). ($C_0 \approx$ 6 ppm for Cs^+, Co^{2+} and Ni^{2+}; V/m = 1000 mL g^{-1}; room temperature).

Water	R^{Cs} (%)	K_d^{Cs} (mL g^{-1})	R^{Co} (%)	K_d^{Co} (mL g^{-1})	R^{Ni} (%)	K_d^{Ni} (mL g^{-1})
DW	99.57	231000	99.01	100138.15	98.91	90480.85
MW	94.23	16336.70	92.78	12860.72	99.44	176938.05
TW	96.08	24504.17	90.80	9869.80	97.91	46820.16
LW	90.29	9299.95	67.65	2091.52	79.51	3879.47
SW	70.73	2415.89	82.07	4577.75	69.77	2307.80

Table S12. Actual pH and concentrations of Na^+, K^+, Mg^{2+} and Ca^{2+} measured in DW, MW, TW, LW and SW. Note: the water samples were taken from the same sources of the following reference, *J. Hazard. Mater.* 2022, 425, 128007.

Water	pH	Na^+ (ppm)	K^+ (ppm)	Mg^{2+} (ppm)	Ca^{2+} (ppm)
DW	6.11	0.38	0.30	0.03	NA
MW	7.83	5.31	3.69	4.35	9.88
TW	7.96	6.16	1.81	4.75	36.3
LW	8.27	683.05	25.05	102.80	81.20
SW	8.10	10781.45	399.10	1283.72	412.08

Table S13. Removal rates and K_d values for mixed Cs^+, Co^{2+} and Ni^{2+} adsorption in presence of individual Al^{3+}, Fe^{3+}, Eu^{3+} and UO_2^{2+} cations ($C_0 \approx 3$ ppm for Cs^+, Co^{2+}, Ni^{2+}, Al^{3+}, Fe^{3+}, Eu^{3+}, UO_2^{2+}; V/m = 1000 mL g^{-1}; room temperature).

Cations	R^{Cs} **(%)**	K_d^{Cs} **(mL g^{-1})**	R^{Co} **(%)**	K_d^{Co} **(mL g^{-1})**	R^{Ni} **(%)**	K_d^{Ni} **(mL g^{-1})**
Al^{3+}	70.45	2384.66	99.42	171206.11	97.59	10738.07
Fe^{3+}	78.71	3695.48	99.02	100887.39	95.29	27897.80
Eu^{3+}	79.89	3971.56	96.88	31018.73	96.54	20240.38
UO_2^{2+}	83.74	5149.50	98.93	92565.96	91.48	40495.27

Table S14. Removal rates and K_d values for mixed Cs^+, Co^{2+} and Ni^{2+} exchange in presence of individual HCO_3^-, NO_3^-, CO_3^{2-}, and SO_4^{2-} anions ($C_0 \approx 3$ ppm for Cs^+, Co^{2+}, Ni^{2+}; $C_0 \approx 30$ ppm for HCO_3^-, CO_3^{2-}, NO_3^- and SO_4^{2-}; V/m = 1000 mL g^{-1}; room temperature).

Anion	R^{Cs} **(%)**	K_d^{Cs} **(mL g^{-1})**	R^{Co} **(%)**	K_d^{Co} **(mL g^{-1})**	R^{Ni} **(%)**	K_d^{Ni} **(mL g^{-1})**
HCO_3^-	79.74	3936.50	86.84	6596.69	86.21	6250.23
NO_3^-	76.29	3218.17	87.72	7146.50	88.31	7557.97
CO_3^{2-}	84.41	5414.95	90.67	9716.46	93.98	15614.45
SO_4^{2-}	77.27	3401.13	86.76	6557.19	87.47	6986.81

Section 5 Elution and reusability

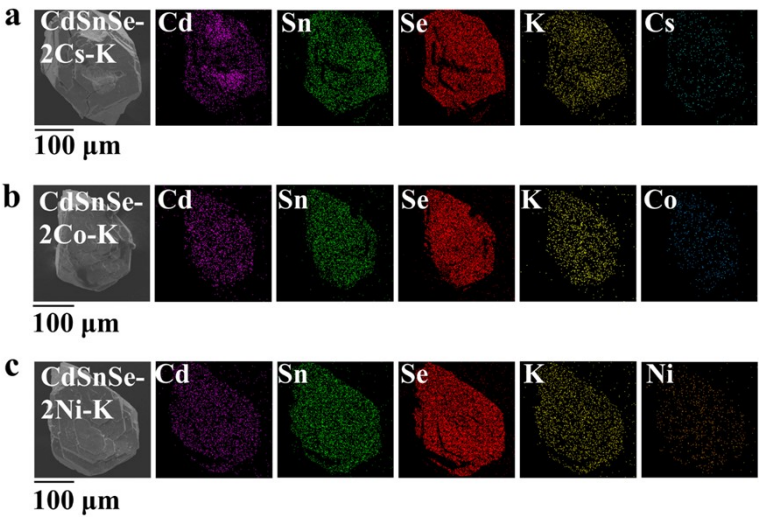

Figure S23. SEM images and elemental distribution maps of the eluted products (a) **CdSnSe-2Cs-K**, (b) **CdSnSe-2Co-K** and (c) **CdSnSe-2Ni-K**.

a

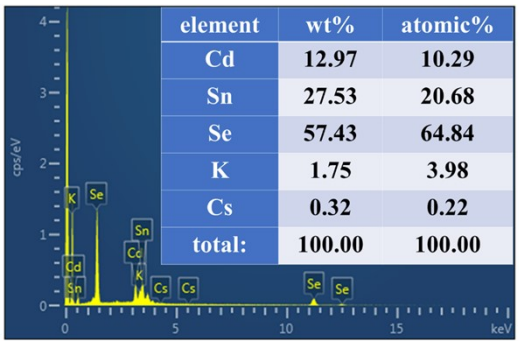

element	wt%	atomic%
Cd	12.97	10.29
Sn	27.53	20.68
Se	57.43	64.84
K	1.75	3.98
Cs	0.32	0.22
total:	100.00	100.00

b

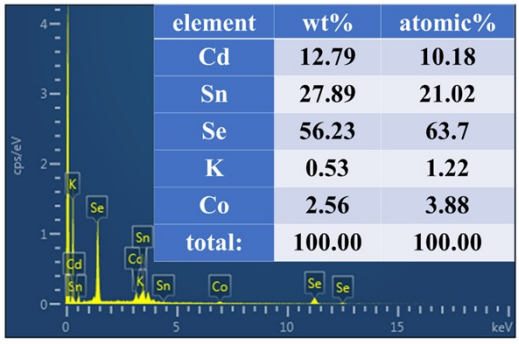

element	wt%	atomic%
Cd	12.79	10.18
Sn	27.89	21.02
Se	56.23	63.7
K	0.53	1.22
Co	2.56	3.88
total:	100.00	100.00

c

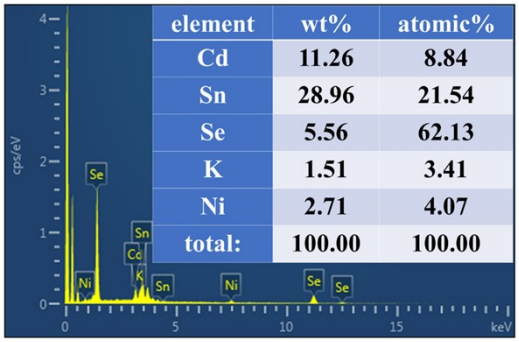

element	wt%	atomic%
Cd	11.26	8.84
Sn	28.96	21.54
Se	5.56	62.13
K	1.51	3.41
Ni	2.71	4.07
total:	100.00	100.00

Figure S24. EDS analyses on the eluted products (a) **CdSnSe-2Cs-K**, (b) **CdSnSe-2Co-K**, and (c) **CdSnSe-2Ni-K**.

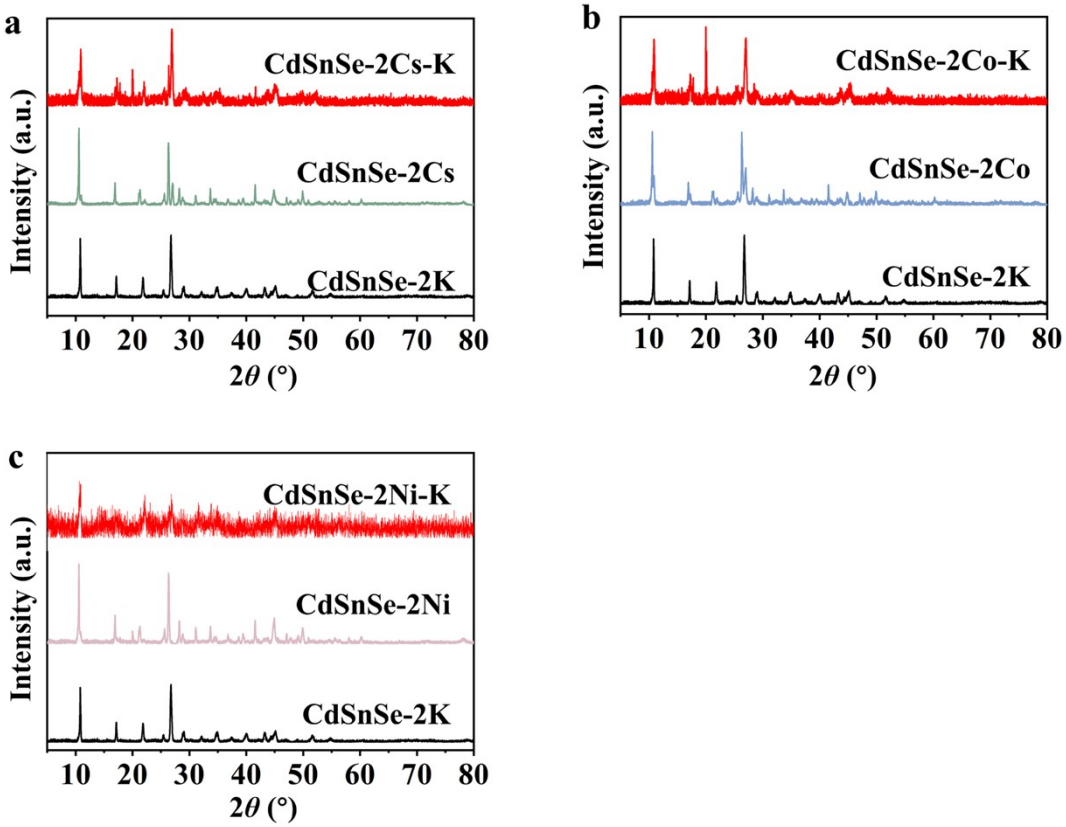

Figure S25. Powder XRD patterns of **CdSnSe-2K**, adsorption-saturated, and eluted products for individual (a) Cs^{+} , (b) Co^{2+} and (c) Ni adsorption.

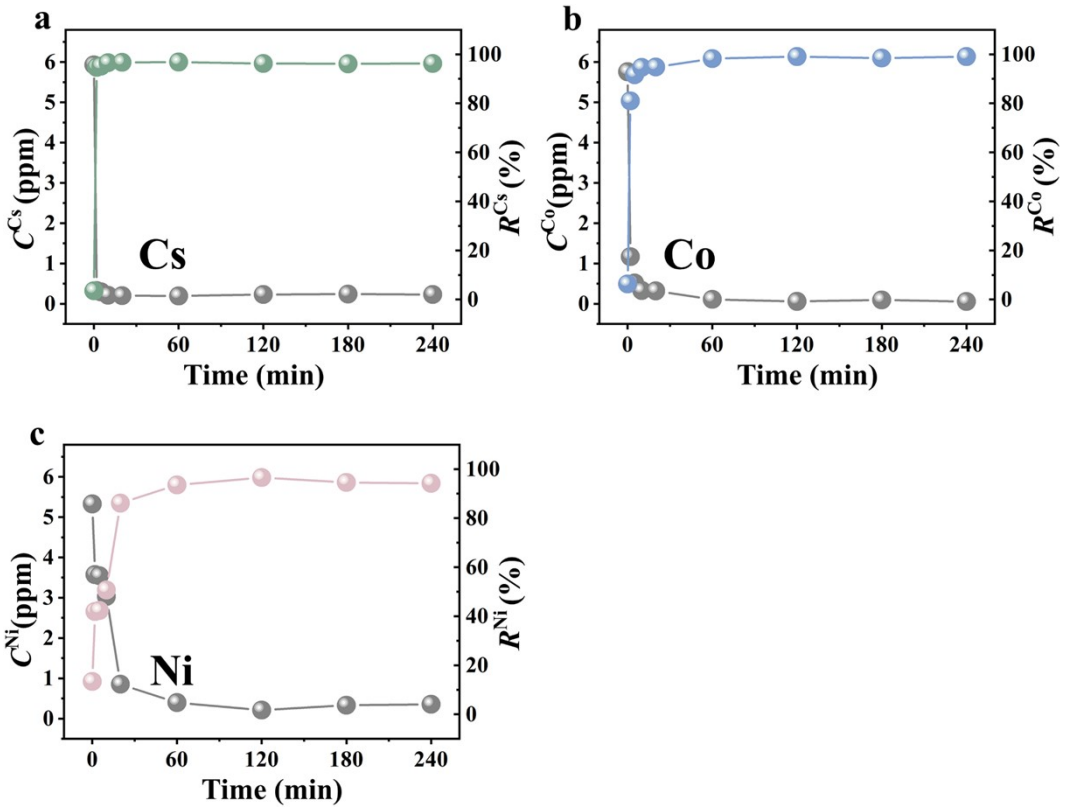

Figure S26. Resorption kinetics curves of Cs^{+}, Co^{2+}, Ni^{2+} by the corresponding eluted products **CdSnSe-2Cs-K**, **CdSnSe-2Co-K** and **CdSnSe-2Ni-K**.

References:

[1] Liu, Y.; Shi, F.-Q.; Hao, X.; Li, M.-Y.; Cheng, L.; Wang, C.; Wang, K.-Y. Open-framework Hybrid Zinc/tin Selenide as an Ultrafast Adsorbent for Cs^+, Ba^{2+}, Co^{2+}, and Ni^{2+}. *J. Hazard. Mater.* **2023**, *458*, 132038.

[2] Zhao, Y.-M.; Cheng, L.; Wang, K.-Y.; Hao, X.; Wang, J.; Zhu, J.-Y.; Sun, M.;Wang, C. pH-Controlled Switch over Coadsorption and Separation for Mixed Cs^+ and Sr^{2+} by an Acid-Resistant Potassium Thioantimonate, *Adv. Funct. Mater.* **2022**, *32*, 2112717.

[3] Tang, J.-H.; Jin, J.-C.; Li, W.-A.; Zeng, X.; Ma, W.; Li, J.-L.; Lv, T.-T.; Peng, Y.-C.; Feng, M.-L.; Huang, X.-Y. Highly Selective Cesium(I) Capture Under Acidic Conditions by a Layered Sulfide. *Nature Commun.* **2022**, *13*, 658.

[4] Jiang, Z.; Ma, C.; He, Y.; Li, M.; Liu, G.; Guo, Y.; Ji, D.; Deng, T. Novel Layered Iron Antimony Thiostannate Adsorbent of $K_{1.61}Fe_{0.04}Sb_{0.03}Sn_{3.1}S_7$ for Cesium Green Recovery from Geothermal Water, *J. Clean. Prod.* **2022**, *347*, 131332.

[5] Rathore, E.; Pal, P.; Biswas, K. Reversible and Efficient Sequestration of Cesium from Water by the Layered Metal Thiophosphate $K_{0.48}Mn_{0.76}PS_3{\cdot}H_2O$. *Chem. Eur. J.* **2017**, *23*, 11085-11092.

[6] Li, J.; Jin, J.; Zou, Y.; Sun, H.; Zeng, X.; Huang, X.; Feng, M.; Kanatzidis, M. G. Efficient Removal of Cs^+ and Sr^{2+} Ions by Granulous $(Me_2NH_2)_{4/3}(Me_3NH)_{2/3}Sn_3S_7{\cdot}1.25H_2O$/Polyacrylonitrile Composite. *ACS Appl. Mater. Interfaces.* **2021**, *13*, 13434-13442.

[7] Manos, M. J.; Kanatzidis, M. G. Highly Efficient and Rapid Cs^+ Uptake by the Layered Metal Sulfide $K_{2x}Mn_xSn_{3-x}S_6$ (KMS-1). *J. Am. Chem. Soc.* **2009**, *131*, 6599-6607.

[8] Sarma, D.; Malliakas, C. D.; Subrahmanyam, K. S.; Islam, S. M.; Kanatzidis, M. G. $K_{2x}Sn_{4-x}S_{8-x}$ (x = 0.65-1): a New Metal Sulfide for Rapid and Selective Removal of Cs^+, Sr^{2+} and UO_2^{2+} ions. *Chem. Sci.* **2016**, *7*, 1121-1132.

[9] Zeng, X.; Zeng, M.; Cai, P.-W.; Tang, J.-H.; Ma, W.; Feng, M.-L.; Huang, X.-Y. Ultra-fast ^{137}Cs Sequestration via a Layered Inorganic Indium Thioantimonate. *Environ. Sci. Adv.* **2022**, *1*, 331-341.

[10] Qi, X.-H.; Du, K.-Z.; Feng, M.-L.; Li, J.-R.; Du, C.-F.; Zhang, B.; Huang, X.-Y. A Two-Dimensionally Microporous Thiostannate with Superior Cs^+ and Sr^{2+} Ion-exchange Property. *J. Mater. Chem. A* **2015**, *3*, 5665-5673.

[11] Li, W.-A.; Li, J.-R.; Zhang, B.; Sun, H.-Y.; Jin, J.-C.; Huang, X.-Y.; Feng, M.-L. Layered Thiostannates with Distinct Arrangements of Mixed Cations for the Selective Capture of Cs^+, Sr^{2+}, and Eu^{3+} Ions. *ACS Appl. Mater. Interfaces* **2021**, *13*, 10191-10201.

[12] Li, J.; Jin, J.; Zhang, T.; Ma, W.; Zeng, X.; Sun, H.; Cheng, M.; Feng, M.; Huang, X. Rapid and Selective Uptake of Cs^+ and Sr^{2+} Ions by a Layered Thiostannate with

Acid–Base and Irradiation Resistances. *ACS EST Water* **2021**, *1*, 2440-2449.

[13] Liao, Y.-Y.; Li, J.-R.; Zhang, B.; Sun, H.-Y.; Ma, W.; Jin, J.-C.; Feng, M.-L.; Huang, X.-Y. Robust and Flexible Thioantimonate Materials for Cs^+ Remediation with Distinctive Structural Transformation: A Clear Insight into the Ion-Exchange Mechanism. *ACS Appl. Mater. Interfaces* **2021**, *13*, 5275-5283.

[14] Gao, Y.-J.; Feng, M.-L.; Zhang, B.; Wu, Z.-F.; Song, Y.; Huang, X.-Y. An Easily Synthesized Microporous Framework Material for the Selective Capture of Radioactive Cs^+ and Sr^{2+} ions. *J. Mater. Chem. A* **2018**, *6*, 3967-3976.

[15] Ma, W.; Lv, T.-T.; Tang, J.-H.; Feng, M.-L.; Huang, X.-Y. Highly Efficient Uptake of Cs^+ by Robust Layered Metal–Organic Frameworks with a Distinctive Ion Exchange Mechanism. *JACS Au* **2022**, *2*, 492-501.

[16] Wang, L.; Pei, H.; Sarma, D.; Zhang, X.-M.; MacRenaris, K.; Malliakas, C. D.; Kanatzidis, M. G. Highly Selective Radioactive $^{137}Cs^+$ Capture in an Open-Framework Oxysulfide Based on Supertetrahedral Cluster. *Chem. Mater.* **2019**, *31*, 1628-1634.

[17] Li, W.-A.; Peng, Y.-C.; Ma, W.; Huang, X.-Y.; Feng, M.-L. Rapid and Selective Removal of Cs^+ and Sr^{2+} Ions by Two Zeolite-type Sulfides via Ion Exchange Method. *Chem. Eng. J.* **2022**, *442* 136377.

[18] El-Kamash, A. M. Evaluation of Zeolite A for the Sorptive Removal of Cs^+ and Sr^{2+} Ions from Aqueous Solutions Using Batch and Fixed Bed Column Operations. *J. Hazard. Mater.* **2008**, *151*, 432-445.

[19] Wu, Y.; Chen, J.; Liu, Z.; Na, P.; Zhang, Z. Removal of Trace Radioactive Cs^+ by Zirconium Titanium Phosphate: From Bench-Scale to Pilot-Scale. *J. Environ. Eng.* **2022**, *10*, 108073.

[20] Mu, W.; Yu, Q.; Li, X.; Wei, H.; Jian, Y. Efficient Removal of Cs^+ and Sr^{2+} from Aqueous Solution Using Hierarchically Structured Hexagonal Tungsten Trioxide Coated Fe_3O_4. *Chem. Eng. J.* **2017**, *319*, 170-178.

[21] Yang, H.; Yu, H.; Sun, J.; Liu, J.; Xia, J.; Fang, J.; Li, Y.; Qu, F.; Song, A.; Wu, T. Facile Synthesis of Mesoporous Magnetic AMP Polyhedric Composites for Rapid and Highly Efficient Separation of Cs^+ from Water. *Chem. Eng. J.* **2017**, *317*, 533-543.

[22] Hu, Y.-y.; Pan, C.; Zheng, X.; Hu, F.; Xu, L.; Xu, G.; Jian, Y.; Peng, X. Prediction and Optimization of Adsorption Properties for Cs^+ on NiSiO@NiAlFe LDHs Hollow Spheres From Aqueous Solution: Kinetics, Isotherms, and BBD Model. *J. Hazard. Mater.* **2021**, *401*, 123374.

[23] Zhao, X.; Meng, Q.; Chen, G.; Wu, Z.; Sun, G.; Yu, G.; Sheng, L.; Weng, H.; Lin, M. An Acid-Resistant Magnetic Nb-Substituted Crystalline Silicotitanate for Selective Separation of Strontium and/or Cesium Ions from Aqueous Solution. *Chem. Eng. J.* **2018**, *352*, 133-142.

[24] Jun, B.-M.; Jang, M.; Park, C. M.; Han, J.; Yoon, Y. Selective Adsorption of Cs^+ by MXene ($Ti_3C_2T_x$) from Model Low-Level Radioactive Wastewater. *Nucl. Eng.*

Technol. **2020**, *52*, 1201-1207.

[25] Datta, S. J.; Moon, W. K.; Choi, D. Y.; Hwang, I. C.; Yoon, K. B. A Novel Vanadosilicate with Hexadeca-Coordinated Cs^+ Ions as a Highly Effective Cs^+ Remover. *Angew. Chem. Int. Ed.* **2014**, *53*, 7203-7208.

[26] Zhang, H.; Li, C.; Chen, X.; Fu, H.; Chen, Y.; Ning, S.; Fujita, T.; Wei, Y.; Wang, X. Layered Ammonium Vanadate Nanobelt as Efficient Adsorbents for Removal of Sr^{2+} and Cs^+ From Contaminated Water. *J. Colloid Interface Sci.* **2022**, *615*, 110-123.

[27] Amesh, P.; Venkatesan, K. A.; Suneesh, A. S.; Maheswari, U. Tuning the Ion Exchange Behavior of Cesium and Strontium on Sodium Iron Titanate. *Sep. Purif. Technol.* **2021**, *267*, 118678.

[28] Chen, S.; Hu, J.; Shi, J.; Wang, M.; Guo, Y.; Li, M.; Duo, J.; Deng, T. Composite Hydrogel Particles Encapsulated Ammonium Molybdophosphate for Efficiently Cesium Selective Removal and Enrichment from Wastewater. *J. Hazard. Mater.* **2019**, *371*, 694-704.